To be appeared in ApJ v554 n2 Jun 20, 2001 issue
Preprint typeset using LaTeX style emulateapj v. 04/03/99

DISCOVERY OF X RAYS FROM CLASS 0 PROTOSTAR CANDIDATES IN OMC-3

Yohko Tsuboi
Department of Astronomy & Astrophysics, 525 Davey Laboratory, Pennsylvania State University, University Park PA 16802, USA
tsuboi@astro.psu.edu

Katsuji Koyama[1], Kenji Hamaguchi
Department of Physics, Faculty of Science, Kyoto University, Sakyo-ku, Kyoto 606-8502, Japan
koyama@cr.scphys.kyoto-u.ac.jp, kenji@cr.scphys.kyoto-u.ac.jp

Ken'ichi Tatematsu, Yutaro Sekimoto
Nobeyama Radio Observatory, National Astronomical Observatory of Japan, Nobeyama, Minamisaku, Nagano 384-1305, JAPAN
tatematsu@nro.nao.ac.jp, sekimoto@nro.nao.ac.jp

John Bally, and Bo Reipurth
Center for Astrophysics and Space Astronomy, University of Colorado, Boulder, CO 80309, USA
bally@casa.colorado.edu, reipurth@casa.colorado.edu

To be appeared in ApJ v554 n2 Jun 20, 2001 issue

ABSTRACT

We have observed the Orion Molecular Clouds 2 and 3 (OMC-2 and OMC-3) with the Chandra X-ray Observatory (CXO). The northern part of OMC-3 is found to be particularly rich in new X-ray features; four hard X-ray sources are located in and along the filament of cloud cores. Two sources coincide positionally with the sub*mm-mm* dust condensations of MMS 2 and 3 or an outflow radio source VLA 1, which are in a very early phase of star formation. The X-ray spectra of these sources show an absorption column of (1–3) $\times 10^{23}$ H cm^{-2}. Assuming a moderate temperature plasma, the X-ray luminosity in the 0.5–10 keV band is estimated to be $\sim 10^{30}$ erg s^{-1} at a distance of 450 pc. From the large absorption, positional coincidence and moderate luminosity, we infer that the hard X-rays are coming from very young stellar objects embedded in the molecular cloud cores.

We found another hard X-ray source near the edge of the dust filament. The extremely high absorption of 3 $\times 10^{23}$ H cm^{-2} indicates that the source must be surrounded by dense gas, suggesting that it is either a YSO in an early accretion phase or a Type II AGN (e.g. a Seyfert 2), although no counterpart is found at any other wavelength.

In contrast to the hard X-ray sources, soft X-ray sources are found spread around the dust filaments, most of which are identified with IR sources in the T Tauri phase.

Subject headings: Stars: coronae— Stars: late-type— Stars: individual (OMC-3)— Stars: protostars— Stars: X-rays— X-rays: spectra

1. INTRODUCTION

Young stellar objects (YSOs) evolve from a molecular cloud core through protostellar and T Tauri phases to a main sequence star. Protostars are generally associated with Class 0 and I energy distributions, peaking in the *mm* and mid-to far infrared wavelengths, respectively. The Class I infrared objects appear to be in a later phase of protostellar evolution.

One of the recent highlights in X-ray studies of YSOs is the discovery of hard X-rays from embedded Class I objects, showing highly absorbed spectra with occasional flares, or even quasi-periodic flaring activity (Koyama et al. 1996, Grosso et al. 1997, Kamata et al. 1997, Tsuboi et al. 2000). The overall X-ray phenomena are consistent with enhanced solar-like magnetic activity, probably generated by a coupled activity of convection and differential rotation on a star or between a star and an inner disk (Tsuboi et al. 2000; Montmerle et al. 2000). X-rays from protostars may be related to the competing processes of accumulation of angular momentum towards the growing central star vs. release of angular momentum by outflow processes. In this context, X-ray observations of Class 0 objects in the dynamical infall phase would be potentially important for the study of protostellar evolution.

The infrared to *mm* radio spectrum of Class 0 objects can be described by a black body model whose temperature is typically 15–30 K (e.g. André, Ward-Thompson, & Barsony 1993). Virtually all the emission is from the surrounding envelope; no emission from a central protostar is seen. Prominent outflows accompany such sources, indicating disk accretion and release of angular momentum from the accreting material. Class 0 protostars may have extremely large absorption, up to 10^{23-24} H cm^{-2} or even more. Therefore hard X-ray imaging is a unique technique to probe the central protostars.

The Orion Molecular Cloud 2 and 3 regions (hereafter OMC-2 and OMC-3), at a distance of about 450 pc (e.g. Genzel & Stutzki 1989) exhibit a chain of Class 0 objects detected at 1300 μm (Chini et al. 1997), 350 μm (Lis et al. 1998), and 450 and 850 μm bands (Johnstone & Bally

[1]CREST, Japan Science and Technology Corporation (JST), 4-1-8 Honmachi, Kawaguchi, Saitama, 332-0012, Japan

1999). The size of the dust condensations is typically 10–50 arcsec (FWHM) which corresponds to 5000–20000 AU (FWHM) at 450 pc distance. The mass of each condensation is estimated to be about 10 $M_{\odot}$, hence could be sites of low to intermediate mass protostars (Chini et al. 1997). Evolution of protostars, from Class 0 to Class I, can be traced from north to south in the clouds: from mainly Class 0 sources in OMC-3 to mainly Class I sources in OMC-2. Consequently, the OMC-2/3 region is a superb place to study Class 0 and Class I sources with the same instrument, and observationally trace the evolution of these protostellar phases.

ASCA observed the OMC-2/3 region (Yamauchi et al. 1996), and hard X-rays (2–10 keV band) are found from the densest regions of the dust filament in the further analysis of the same data by Tsuboi (1999). The hard X-ray distribution is well correlated with both the ridge of molecular clouds and the cold dust condensations (1300 μm and 350 μm peaks) within the limited spatial resolution of ASCA. No excess in the soft X-ray band (0.7–2 keV) is found from the OMC-3 region. Stimulated by this suggestion of hard X-ray emission from inside the dust condensations (1300 μm and 350 μm peaks), and in order to find X-ray emission from Class 0 sources, we have carried out Cycle 1 Chandra observations with more than 100 times better spatial resolution than ASCA. This paper presents a first report on the highlights of the new Chandra observations detecting hard X-ray emission from the north of OMC-3, a site of the youngest protostellar objects.

2. OBSERVATIONS AND DATA REDUCTION

The OMC-2/3 observation was made in the New Year days of the new millennium (2000 January 1–2) with the Chandra X-ray Observatory (CXO) for 89.2 ks, having wide band sensitivity in the 0.2–10 keV energy range with moderate energy resolving power and particularly high spatial (sub-arcsec) resolution at the on-axis position. We used the ACIS-I array consisting of four abutted X-ray CCDs, which covers the complete OMC-2 and OMC-3 clouds, and one CCD from the ACIS-S array covering a small region north of OMC-3. In this paper we focus on and discuss the data towards the northern part of OMC-3, which were recorded with one of the ACIS-I CCDs.

We used Level 1 processed events provided by the pipeline processing at the Chandra X-ray Center. To minimize the effect of the degradation of charge transfer inefficiency (CTI), we applied the improved data processing technique developed by Townsley et al. (2000). To reject background events, we applied a grade filter to keep only *ASCA* grades[2] 0, 2, 3, 4, & 6. We removed events from flaring pixels using the "flagflare" routine written by T. Miyaji. Artificial stripes caused probably by hot pixels in the frame-store region and by particles which hit on the CCD node boundaries were also removed. Detailed procedures for cleaning low-quality events are given in *http://www.astro.psu.edu/xray/axaf/recipes/clean.html*.

3. RESULTS

3.1. *X-ray positions and identifications*

Figure 1 shows a $2' \times 3'$ field image around the northern part of OMC-3 in the 0.5–6 keV band overlaid with the 1300 μm emission contour map from Chini et al. (1997). Red color represents photon energies below 3 keV, while blue represents hard photons above 4 keV energy. The absolute coordinates of the X-ray images are fine-tuned to better than 0.1 arcsec, using the 2MASS infrared source catalog 2MASS, of which details are given below.

For source finding, we used the *wavdetect* program in the Chandra Interactive Analysis of Observations Software (CIAO[3], Version 1.0), which is based on a Mexican hat wavelet decomposition and reconstruction of the image (Freeman et al. 2000). We set the significance criterion at 1×10^{-5} and wavelet scales ranging from 1 to 16 pixels in multiples of $\sqrt{2}$. The source detection was performed separately in the soft (0.5–2 keV), hard (2–8 keV), and total (0.5–8 keV) bands to improve sensitivity for non-embedded (soft X-ray band), embedded (hard), and mildly embedded faint (total) sources, respectively. In the 0.5–2 keV band, the contribution of the ASCA grade 6 to the photons of point sources is about 1 %, while that to background is about 8 % in the same band. In order to maximize the signal-to-noise ratio, we hence used only the ASCA grades 0, 2, 3 and 4 for the source finding in the soft (0.5–2 keV) band, while the ASCA grades 0, 2, 3, 4 and 6 are used in the other bands.

In the field shown in Figure 1, the source finding algorithm picked up thirteen sources (No. 1–13 in Table 1) above a 4 σ significance level in either of the three bands. We compared these sources to the optical star catalog Hipparcos, and the infrared catalog 2MASS. Only one counterpart is found from the optical catalog, while two thirds of the sources have counterparts in the 2MASS catalog. Selecting the five brightest X-ray sources, with statistical errors within 0.3 arcsec at 90 % confidence, we have made a cross-correlation to the 2MASS infrared candidates, weighting by photon counts. This resulted in a $1''.1$ bore-sight correction to the ACIS field; ACIS sources had offsets of $+0''.51$ and $-0''.95$ for right ascension and declination from the 2MASS frame, respectively. After the coordinate correction, the systematic astrometric accuracy becomes better than 0.1 arcsec at 90 % confidence. The thus corrected X-ray positions, counts in the 0.5–8 keV band, and hardness ratio are listed in Table 1, together with the J, H, and K magnitudes of the infrared counterparts and the offset angle between the X-ray and IR positions. Since the offsets and nominal absolute errors of the 2MASS sources are about 0.1–0.3 arcsec and 0.1 arcsec, our X-ray position errors of sources No. 1–13 should be 0.1–0.4 arcsec.

From figure 1, we see the hard X-ray sources more concentrated to the dust emission in the 1300 μm band (Chini et al. 1997). Among the hard X-ray sources, two sources (No. 8 and 10 in Table 1) coincide with positions of the dust condensations MMS 2 and MMS 3[4] (Chini et al. 1997) and CSO 6 and CSO 7 (Lis et al. 1998) within position errors of $\sim 5''$.

[2]see http;//asc.harvard.edu/udocs/docs/POG/MPOG/index.html

[3]available at http;//asc.harvard.edu/ciao/

[4]The coordinates of MMS 3 given in Table 1 of Chini et al. was incorrect due to their problem in a Gaussian fit. Then we referred the correct coordinate $\alpha = 5^h32^m51.3^s$, $\delta = -5^d02^m44.3^s$ in B1950 (Sievers A. private communication).

We further checked the hard X-ray enhancements from the other Class 0 protostar candidates or the dust condensations in the field of Figure 1. The 2–8 keV band photon fluxes in a $5''$ radius circle around the 1300 μm (MMS 1–4, Chini et al. 1997) and 350 μm (CSO 4–8, Lis et al. 1998) sources are all below 3 σ significance level except for MMS 2 (= CSO 6) and MMS 3 (= CSO 7).

Since we found a complex structure around source No. 8, we made closed-up views near this source in the 0.5–3 keV and 3–6 keV bands, which are shown in figure 2. The position of 2MASS sources are indicated by crosses. In the close vicinity of source No. 8, we can clearly see one source in the 0.5–3 keV and two sources in the 3–6 keV band, although the source finding algorithm has missed them. We here refer to these sources as a, b, and c, as indicated in Figure 2. The X-ray positions are listed in Table 1. Neither optical nor IR counterparts are found towards the hard band sources a and b, but the soft band source c coincides with a 2MASS source with the J, H, and K magnitudes of >16.9, >15.2, and 11.4, respectively.

3.2. *X-ray spectra*

3.2.1. *Bright Sources*

The brightest five sources in Figure 1 have reasonable statistics (more than 100 photons), and we therefore made the X-ray spectra by selecting $4''$–$9''$ radius circles around the sources to include ∼99 % and ∼90 % photons at 1.5 keV and 10 keV, respectively. The background spectra are made from an annulus with inner and outer radii of 1.0 and 1.3 times of the source radius, respectively. We fitted the background subtracted spectra with a thin thermal plasma model (MEKAL model; Mewe, Gronenschild, & van den Oord 1985, Mewe, Lemen, & van den Oord 1986, Liedahl, Osterheld, & Goldstein 1995) with interstellar absorption. The effective area of the telescope mirrors and the detection efficiency of ACIS were calculated with the *mkarf* program in CIAO, Version 1.0. In the fitting, we fixed the abundances to 0.3 solar, referring to the results for many YSOs in various star forming regions obtained from the earlier ASCA observations (ex. Orion: Yamauchi et al. 1996, Rho Oph: Kamata et al. 1997). The best fit values are listed in Table 2.

In order to justify our spectra fitting procedure, we selected the ASCA target No. 7 in Yamauchi et al. (1996) and compared our Chandra results. This source lies 9 arc-min south-east from the center of Figure 1. Both our result and that in Yamauchi et al. (1996) are in reasonable agreement; the temperature, abundance, and the absorbing column, are 2.7 vs. 2.2 keV, 0.19 vs. 0.20 solar, and 1.1×10^{21} vs. 0.8×10^{21} H cm^2 (we referred to the 1-temperature model obtained with SIS and GIS simultaneous fitting in Yamauchi et al. 1996). Therefore even with significant calibration uncertainties in the early phase of the CXO observations, our fitting gives reliable results.

3.2.2. *Hard X-ray Sources*

Although the statistics are limited, we examined spectra of the new hard X-ray sources No. 8, 10 and 11. To minimize contamination from the three sources (a, b and c) located in the close vicinity of source No. 8, we extracted the spectrum for No. 8 from a small circle of 2 arcsec radius centered on No. 8. Then now, the contamination from sources a and b to the region is negligible. As for No. 10 and 11, we also used the same radius circles in order to treat the hard source spectra uniformly. Using the software package XSPEC[5] and MARX[6] (version 3.01), we calculated the effective area for this region smaller than the Chandra Point Spread Function at the off-axis position of these sources. These small regions include a background of at most 1 photon, hence we made no background subtraction for these hard sources.

The spectra of No. 10 and 11 are fitted with a thin thermal plasma model (MEKAL model) with 0.3 solar abundance and absorption. However, essentially no constraints on the temperature and absorption are obtained, since these two parameters are strongly coupled. We hence fixed the temperature at two extremes, 1 and 5 keV, referring the best fit temperature of the soft sources. The absorptions are constrained to be larger than 10^{23} H cm^{-2}. We next assumed the temperature to be 3.2 keV, because the hardest source (No. 12) among the bright five has 3.2 keV plasma, and previous results towards very young stars (Class I) are more or less around this value. The best-fit spectra and parameters are shown in Figure 3 (b) and (c) and listed in Table 2.

Figure 3 (a) indicates the spectrum obtained from the circle centered on No. 8. It is more complicated than the others, showing a flux minimum at about 3 keV, which implies the presence of two spectral components: one is hard and heavily absorbed component (dashed line) from No. 8 and the other is soft and less absorbed component that is contamination from the source c (dash-dotted line) separated from No. 8 by $2''$. Then we fitted the spectrum with two thin thermal plasma (MEKAL model) components with independent absorptions. Since the 2MASS counterpart of source c has flux ratios in J, H, and K consistent with those of source No. 12, we assumed the X-ray temperature and absorption for the contamination from c (soft component) to be the same as those of No. 12. The absorption of the hard component is found to be larger than 10^{23} H cm^{-2}, with weak dependence on the assumed temperature (1 and 5 keV). In Table 2, we give the best-fit model in which we assume the temperature of the hard component to be 3.2 keV. The lower energy component is exactly the same as that of spill-over photons from c to the source region of No. 8 (3 counts) which was predicted by simulation with XSPEC and MARX.

3.3. *Time Variability*

To obtain temporal variations of individual X-ray sources, we applied a Kolmogorov-Smirnov test under the assumption of constant flux for individual sources using the XRONOS[7] (Ver. 4.02) software package. The results are listed in Table 1. Among the sources, only one source (source No. 9 in Table 1) exhibited a clear flare.

[5]http://xspec.gsfc.nasa.gov/

[6]http://spce.mit.edu/ASC/MARX

[7]http://xronos.gsfc.nasa.gov/

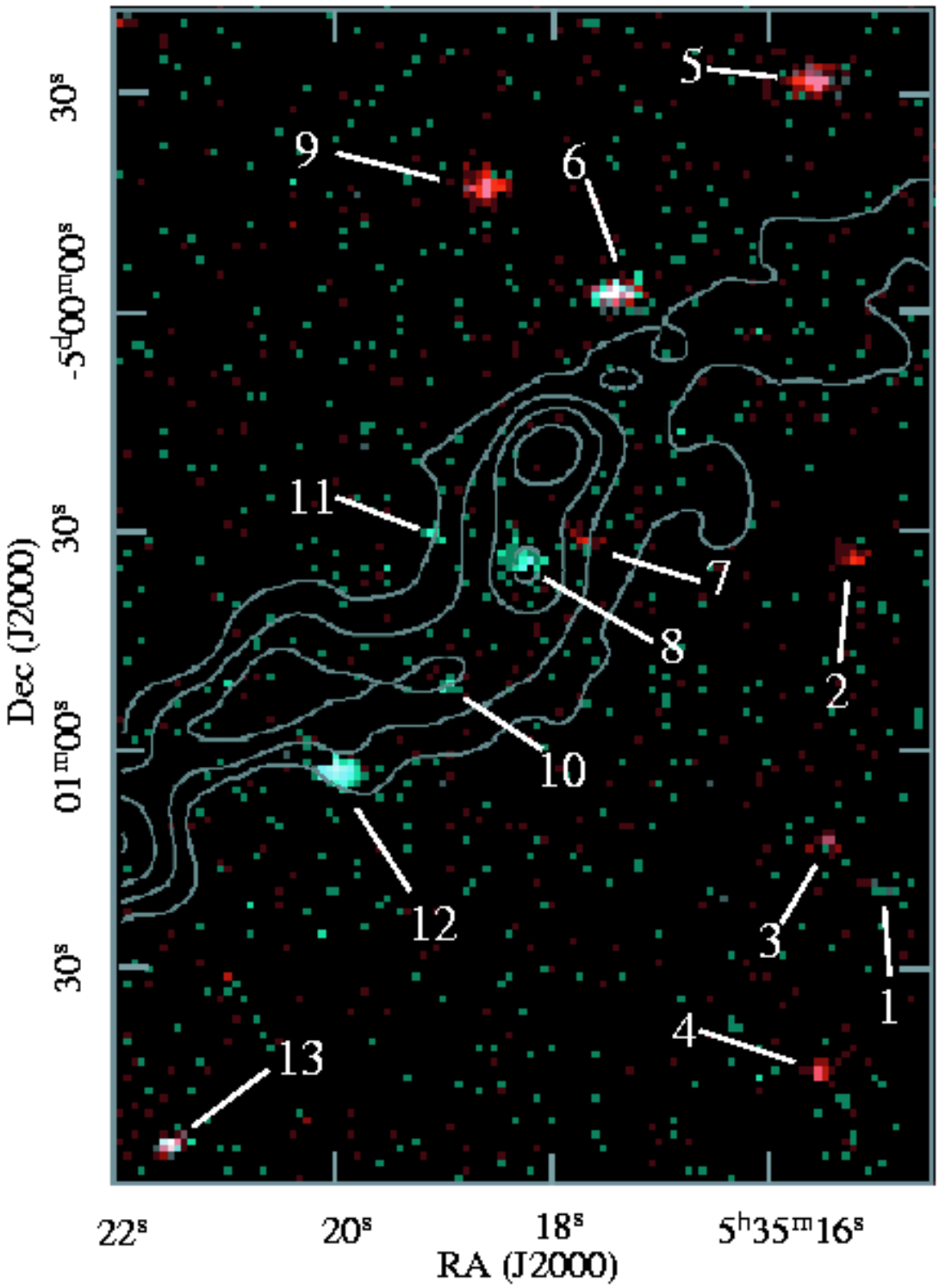

FIG. 1.— A $2' \times 3'$ field image around the northern part of OMC-3 in the 0.5–6 keV band overlaid with a 1300 μm emission contour map from Chini et al. (1997). Red color represents the photon energy below 3 keV, while blue represents hard photons above 4 keV energy. The absolute coordinates of the X-ray images have been fine-tuned to better than 0.1 arcsec, by reference to the 2MASS infrared source catalog (see the text). Source numbers in table 1 are labeled.

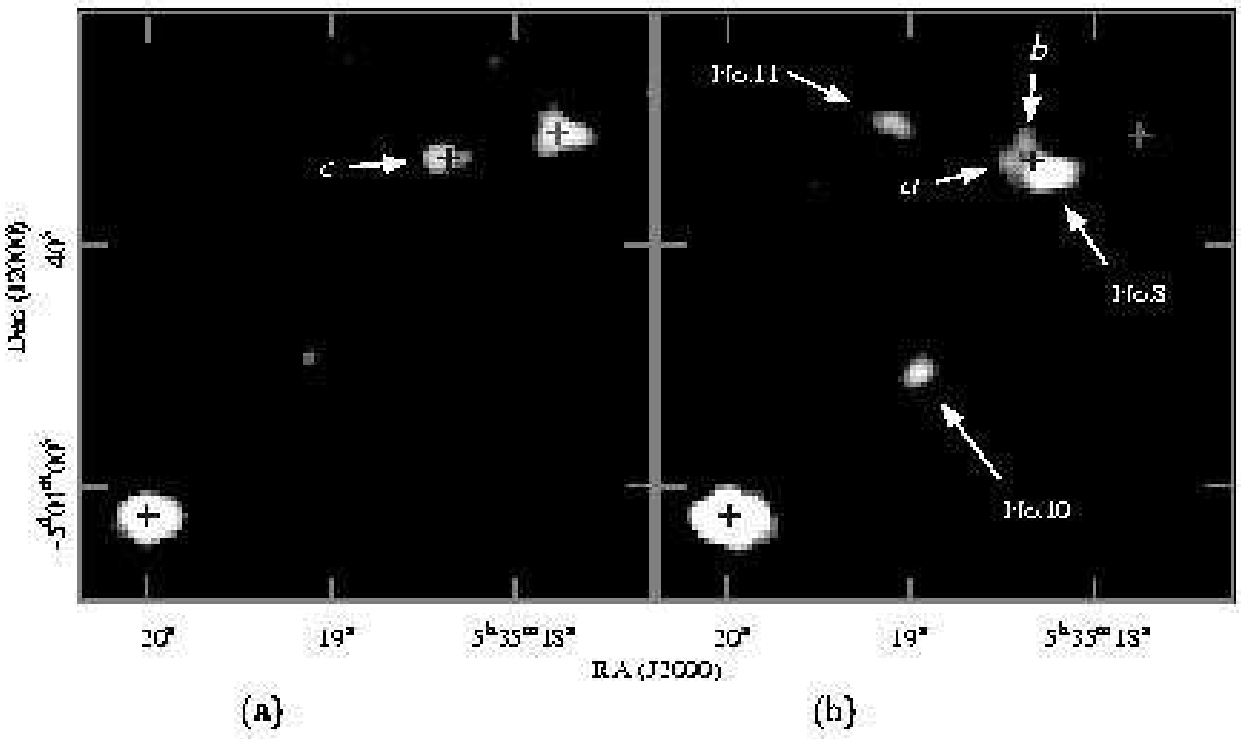

FIG. 2.— Closed-up views near the source No. 8 in the 0.5–3 keV (right panel) and 3–6 keV bands (left panel). The position of 2MASS sources are indicated by crosses. Neither optical nor IR counterparts are found at the hard band sources *a* and *b*, but the soft band source *c* coincides with the position of a 2MASS source.

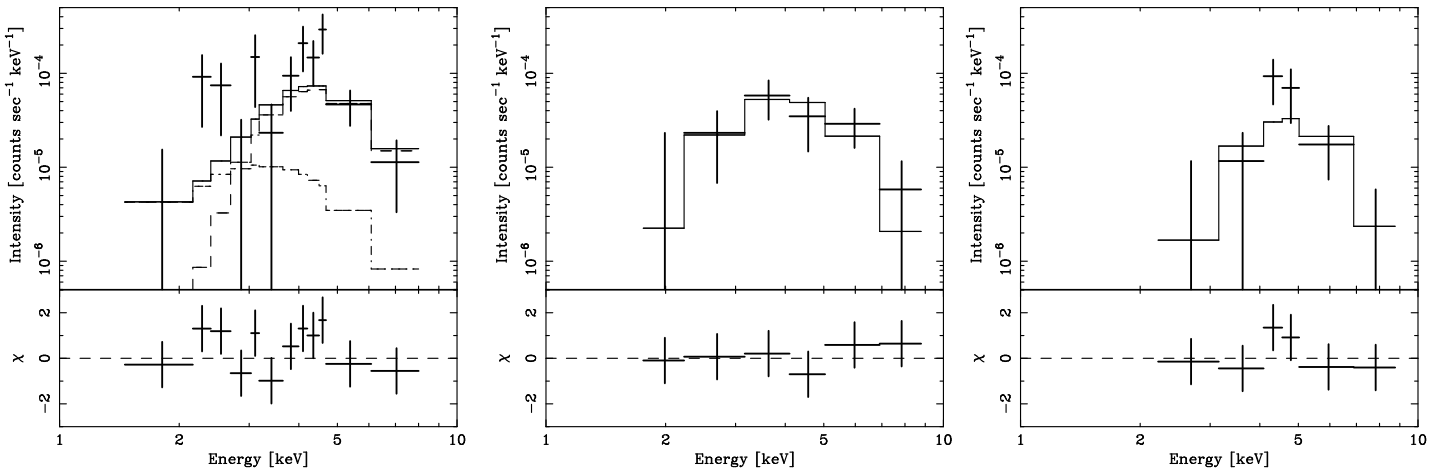

FIG. 3.— The spectra extracted from a circle of 2 arcsec radius centered on No. 8 (figure 3a), 10 (figure 3b) and 11 (figure 3c). The spectrum shown in figure 3a contains two components; one is hard and heavily absorbed component (dashed line) from source No. 8 and the other is soft and less absorbed component that is contamination from source *c* (dash-dotted line). Sources No. 10 and 11 are fitted with a coronal plasma model (MEKAL model). The lower panel shows the residuals from the best-fit model.

4. DISCUSSION

We have detected about one dozen X-ray sources in the northern part of OMC-3. This region has been observed in X rays with *Einstein* (Ku & Chanan 1979, Vaiana et al. 1981, Caillault & Zoonematkermani 1989, Gagné et al. 1994), with *ROSAT* (Gagné et al. 1995, Alcalá et al. 1996) and with *ASCA* (Yamauchi et al. 1996), however, no X-ray sources has been detected in the previous observations. Then all the X-ray sources in Table 1 are new X-ray objects. All the soft band sources (hardness ratios in Table 1 are less than 0.2; No. 5, 6, 9, 12, and 13) have IR counterparts, most of which are likely to be TTSs. The X-ray properties of the the soft band sources, i.e., plasma temperatures (a few keV), luminosities (10^{30} erg s^{-1}), and time variabilities including the detection of a flare (for source No. 9) are consistent with those of TTSs previously reported (ex. Kamata et al. 1997).

The most notable result is the discovery of the highly absorbed X-ray sources No. 8 and 10 coincident within the absolute position error of $\sim 5''$ with the dust condensations MMS 2 (= CSO 6) and MMS 3 (= CSO 7). Since the background X-ray source density above the present detection limit (10^{-14} erg cm^{-1} s^{-1}) is about 1 source $arcmin^{-2}$, the probability to detect an X-ray source by chance within the error circle of the millimeter sources (5 arcsec radius circle) is about 2 %. On the other hand, Reipurth, Rodríguez, & Chini (1999) found a VLA source (VLA 1) towards MMS 2 with absolute position accuracy of $1''$. It is only $1''.4$ apart from the source No. 8, hence these are certainly associated with each other. Together with the large column of No. 8 and No. 10 of 1–3 $\times 10^{23}$ H cm^{-2}, we therefore conclude that the hard X-ray sources No. 8 and 10 are located in the dust condensations MMS 2 and 3.

The flux ratios of 350 μm to 1300 μm for MMS 2 (= CSO 6) and MMS 3 (= CSO 7) are 99 and 87[8], respectively, which are somewhat larger than the average of the other MMS sources in OMC-3. However, no systematic trends are apparent. The MMS 3 seems to be associated with a shock-excited H_2 flow D (Yu, Bally, & Devine 1997), plotting the correct coordinate (Sievers A. private communication) on Figure 4 of Yu et al. (1997). MMS 2 is associated with a prominent H_2 flow B (Yu, Bally, & Devine 1997), a Herbig-Haro object HH 331 (Reipurth 1999), molecular outflow (^{12}CO $J = 2 - 1$, Yu et al. 2000), and 3.6 cm emission (VLA 1, Reipurth, Rodríguez & Chini 1999), which is most likely due to a thermal jet. In addition, Aso et al. (2000) detected unresolved HCO^+ outflow around MMS2–4 region. Given these powerful outflow activities and considering that the two sources are parts of a chain of similar sources of which at least six are documented Class 0 sources, MMS 2 and 3 are most probably also Class 0 sources. Besides them, the absorption columns of MMS 2 and 3 obtained by our observation ($> 10^{23}$ cm^{-2}) are one order of magnitudes larger than those of Class I protostars obtained with ASCA (Kamata et al. 1997, Tsuboi et al. 2000) and Chandra (Imanishi, Koyama & Tsuboi 2001), which highly supports that they are Class 0 sources. Therefore it is likely that this is the first discovery of X-rays from YSOs preceding the Class I phase.

No significant X-ray enhancement is found from other dust condensations than MMS 2 and 3 in the northern part of OMC-3. One may attribute it to much more larger columns (larger mass) than for MMS 2 and 3, but simple estimates based on the mass and size suggest that the column densities of them are 10^{23}–10^{24} H cm^{-2}, and no systematic difference from MMS 2 and 3 are seen.

The soft source *c* is probably unrelated to the MMS 2 condensation, and may be located in front. However, the hard sources *a* and *b* are likely to be located within the MMS 2 core. If this is so, the MMS 2 core is a site of multiple star formation.

Source No. 11, although located at the edge of the dust filament, exhibits a large absorption of 3×10^{23} H cm^{-2}, which exceeds the expected column of the cloud at this position. Thus the large absorption should be very local to the source No. 11, possibly either infalling gas around a protostar (protostellar scenario) or a torus surrounding an active galactic nucleus (type II AGN scenario).

We express our thanks to the High-energy Astrophysics Group at the Penn State University led by Prof. G. Garmire. Most of the data reduction procedure and analysis were made using the software packages and methods developed by this team. We also gratefully acknowledge the assistance of Prof. E. D. Feigelson, Dr. Y. Maeda, and Dr. L. Townsley. We are grateful to Dr. A. Sievers for information about 1300 *mum* emission from MMS 3. A part of this work is supported by the JPS grant of collaboration with foreign country (grant No. 10147103). YT is financially supported by JSPS.

Reference

Andre, P., Ward-Thompson, D. & Barsony, M. 1993, ApJ 406, 122

Aso, Y., Tatematsu, K., Sekimoto, Y., Nakano, T., Umemoto, T., Koyama, K., Yamamoto, S. 2000, ApJS in press

Caillault, J-P & Zoonematkermani, S. 1989, ApJL 338, L57

Chini, R., Reipurth, Bo., Ward-Thompson, D., Bally, J., Nyman, L-A, Sievers, A., & Billawala, Y., 1997, ApJ 474, L135

Freeman, P. E., Kashyap, V., Rosner, R., & Lamb, D. Q. 2000, ApJ, submitted

Gagne, M. & Caillault, J-P. 1994, ApJ 437, 361

Gagne, M., Caillault, J-P., & Stauffer, J. R., 1995 ApJ 445, 280

Genzel, R. & Stutzki, J. 1989, ARA&A 27, 41

Grosso, N., Montmerle, T., Feigelson, E. D., Andre, P., Casanova, S., & Gregorio-Hetem, J. 1997, Nature 387, 56

Imanishi, K., Koyama, K., & Tsuboi, Y. 2001 in preparation

Johnstone, D. & Bally, J. 1999, ApJL 510, L49

Kamata, Y., Koyama, K., Tsuboi, Y., & Yamauchi, S. 1997, PASJ 49, 461

Koyama, K., Hamaguchi, K., Ueno, S., Kobayashi, N., & Feigelson. E. 1996, PASJ 48, L87

Ku W. H.-M. & Chanan, G. A. 1979, ApJL 234, L59

Liedahl, D. A., Osterheld, A. L., Goldstein, W. H. ApJL 438, 115

[8]The peak flux density of MMS 3 in Table 1 in Chini et al. 1997 was incorrect. Then we referred the correct flux 300 mJy (Sievers A. private communication).

Lis, D. C., Serabyn, E., Keene, Jocelyn, Dowell, C. D., Benford, D. J., Phillips, T. G., Hunter, T. R., & Wang, N. 1998, ApJ 509, 299

Mewe, R., Gronenschild, E. H. B. M., & van den Oord, G. H. J. 1985, A&AS 62, 197

Mewe, R., Lemen, J. R, & van den Oord, G. H. J. 1986, A&AS 65, 511

Montmerle, T., Grosso, N., Tsuboi, Y., & Koyama, K. 2000, ApJ 532, 1089

Reipurth, B. 1999, *A General Catalogue of Herbig-Haro Objects*, 2. Edition, available at http://casa.colorado.edu/hhcat

Reipurth, B., Rodríguez, L. F., & Chini, R. 1999, ApJ 118, 983

Townsley, L. K., Broos, P. S., Garmire, G. P., & Nousek, J. A. 2000, ApJL 534, L139

Tsuboi, Y., Imanishi, K., Koyama, K., Grosso, N., & Montmerle, T. 2000, ApJ 532, 1097

Tsuboi, Y. 1999, PhD thesis, see also ISAS RN 689

Vaiana, G. S., Fabbiano, G., Giacconi, R., Golub, L., Gorenstein, P., Harnden, F. R. Jr., Cassinelli, J. P., Haisch, B. M., Johnson, H. M., Linsky, J. L., Maxson, C. W., Mewe, R., Rosner, R., Seward, F., Topka, K., & Zwaan, C. 1981, ApJ 245, 163

Yamauchi, S., Koyama, K., Sakano, M., & Okada, K. 1996, PASJ 48, 719

Yu, K. C., Bally, J., & Devine, D. 1997, ApJL 485 L45

Yu, K. C., Billawala, Y., Smith, M. D., Bally, J., Butner, H. M. 2000, AJ in press

TABLE 1
ACIS SOURCES IN NORTHERN PART OF OMC-3.

#	ACIS sources					counterparts									
	R.A.[a]	Dec[a]	Cnts[b]	HR[c]	V.P.[d]	infrared[e]				submm[f]		mm[g]		cm[h]	
					[%]	θ [$''$]	J	H	K	θ [$''$]		θ [$''$]		θ [$''$]	
1	5 35 14.92	−5 01 18.7	18	0.78±0.27	45	···	···	···	···	···	···	···	···	···	···
2	5 35 15.26	−5 00 33.2	26	−1.00±0.14	49	0.3	13.4	12.8	12.5	···	···	···	···	···	···
3	5 35 15.49	−5 01 12.5	21	−0.43±0.28	77	0.3	14.4	13.7	13.3	···	···	···	···	···	···
4	5 35 15.56	−5 01 43.9	33	−0.58±0.20	99.5	0.2	13.7	12.6	12.0	···	···	···	···	···	···
5	5 35 15.59	−4 59 27.8	146	−0.44±0.09	94	0.2	14.8	12.8	11.6	···	···	···	···	···	···
6	5 35 17.42	−4 59 57.2	253	0.18±0.07	99.9	0.1	>16.8	14.7	12.9	···	···	···	···	···	···
7	5 35 17.73	−5 00 30.9	26	−0.31±0.25	99.4	0.1	15.5	13.1	11.7	···	···	···	···	···	···
8	5 35 18.22	−5 00 34.0	28	1.00±0.13	66	···	···	···	···	5.9	CSO 6	1.5	MMS 2	1.4	VLA 1
a	5 35 18.37	−5 00 31.9	5	1.00±0.75	76	···	···	···	···	2.9	CSO 6	3.1	MMS 2	···	···
b	5 35 18.45	−5 00 33.4	7	1.00±0.53	72	···	···	···	···	3.7	CSO 6	2.5	MMS 2	···	···
c	5 35 18.37	−5 00 32.9	11	1.00±0.34	97	0.6	>16.9	>15.2	11.4	(3.7	CSO 6)*	(2.1	MMS 2)*	(1.0	VLA 1)*
9	5 35 18.61	−4 59 42.5	158	−0.78±0.06	>99.9[†]	0.2	13.8	13.2	13.0	···	···	···	···	···	···
10	5 35 18.93	−5 00 51.0	17	0.88±0.26	79	···	···	···	···	4.2	CSO 7	4.2[‡]	MMS 3	···	···
11	5 35 19.08	−5 00 30.2	13	0.85±0.33	81	···	···	···	···	···	···	···	···	···	···
12	5 35 19.98	−5 01 02.8	262	0.89±0.04	98	0.1	>18.4	>17.4	14.5	···	···	···	···	···	···
13	5 35 21.50	−5 01 53.9	93	0.05±0.12	95	0.2	>18.4	15.4	13.2	···	···	···	···	···	···

[a] Coordinates in J2000.

[b] Background-subtracted counts in 0.5–8 keV band.

[c] Hardness ratios defined as $Z_h - Z_s$ / $Z_h + Z_s$ at which Z_h, Z_s are the count rates in the hard band (2.0–8.0 keV) and soft band (0.5–8 keV), respectively.

[d] Variability probability obtained by the Kolmogorov-Smirnov test to X-ray fluxes in the 0.5–8 keV band with XANADU/XRONOS package version 4.02.

[e] 2MASS counterparts. Offsets from the ACIS sources θ and J, H, and K magnitudes are shown. Lower limit for the magnitudes are 95% confidence level.

[f] Counterparts in 350 μm band (Lis et al. 1998).

[g] Counterparts in 1300 μm band (Chini et al. 1997).

[h] Counterparts in 3.6 cm band (Reipurth, Rodríigues, and Chini 1998).

*This source lies within the positional error of CSO 6=MMS 2=VLA 1, but would be unrelated to the core and located in front. See the text.

[†] A flare is seen in this light curve.

[‡] We obtained this offset referring corrected coordinate of MMS 3 by Sievers A. (private communication). See the footnote in text.

TABLE 2

BEST-FIT PARAMETERS TO THE SPECTRA OF THE ACIS SOURCES IN NORTHERN PART OF OMC-3.

ACIS sources #	kT [keV]		E.M.[a] [10^{52} cm^{-3}]		$N_{\rm H}$ [10^{22} H cm^{-2}]		flux[b] [10^{-15} ergs cm^{-2} s^{-1}]	$L_{\rm X}$[c] [10^{29} ergs s^{-1}]	χ^2 / d.o.f
5	1.5	(0.6–2.1)	9	(4–58)	1.0	(0.6–2.1)	11	8	18/14
6	1.6	(1.2–2.0)	40	(24–71)	2.5	(2.0–3.2)	33	40	10/25
8[†]	3.2	(fix)	21	(8–41)	25	(12–54)	13	20	12/10
9	1.6	(1.2–2.3)	2.5	(2.0–2.9)	0.0	(0.0–0.1)	9	2	15/14
10	3.2	(fix)	9	(3–22)	14	(7–34)	8	10	1/4
11	3.2	(fix)	14	(3–39)	33	(15–69)	8	20	3/4
12	3.2	(2.1–6.8)	43	(23–88)	6	(4–8)	63	50	20/25
13	2.0	(1.1–5.5)	10	(4–31)	2.3	(1.5–3.6)	13	10	8/9

NOTE.—The errors are at 90% confidence level, and metal abundance is fixed to 0.3 solar.

[a]Emission Measure, $\int n_e^2 dV$ (n_e: electron density, V: emitting volume)

[b]Flux in 0.5 – 10 keV band.

[c]Absorption-corrected X-ray luminosity in 0.5 – 10 keV band.

[†]Hard component of the two temperature model (see the text).